Published in final edited form as:

Cell. 2015 August 13; 162(4): 849–859. doi:10.1016/j.cell.2015.07.012.

Mechanistic Origin of Microtubule Dynamic Instability and Its Modulation by EB Proteins

Rui Zhang[1], **Gregory M. Alushin**[2,5], **Alan Brown**[4], and **Eva Nogales**[1,3,*]

[1]Life Sciences Division, Lawrence Berkeley National Laboratory, Berkeley, CA 94720, USA

[2]Biophysics Graduate Program, University of California, Berkeley, Berkeley, CA 94720, USA

[3]Department of Molecular and Cell Biology, Howard Hughes Medical Institute, University of California, Berkeley, Berkeley, CA 94720, USA

[4]MRC Laboratory of Molecular Biology, Francis Crick Avenue, Cambridge CB2 0QH, UK

SUMMARY

Microtubule (MT) dynamic instability is driven by GTP hydrolysis and regulated by microtubule-associated proteins, including the plus-end tracking end-binding protein (EB) family. We report six cryo-electron microscopy (cryo-EM) structures of MTs, at 3.5 Å or better resolution, bound to GMPCPP, GTPγS, or GDP, either decorated with kinesin motor domain after polymerization or copolymerized with EB3. Subtle changes around the E-site nucleotide during hydrolysis trigger conformational changes in α-tubulin around an "anchor point," leading to global lattice rearrangements and strain generation. Unlike the extended lattice of the GMPCPP-MT, the EB3-bound GTPγS-MT has a compacted lattice that differs in lattice twist from that of the also compacted GDP-MT. These results and the observation that EB3 promotes rapid hydrolysis of GMPCPP suggest that EB proteins modulate structural transitions at growing MT ends by recognizing and promoting an intermediate state generated during GTP hydrolysis. Our findings explain both EBs end-tracking behavior and their effect on microtubule dynamics.

Graphical Abstract

*Correspondence: enogales@lbl.gov.

[5]Present address: Cell Biology and Physiology Center, National Heart Lung and Blood Institute, Bethesda, MD 20892, USA

ACCESSION NUMBERS

The following cryo-EM maps and refined atomic models (accession numbers indicated) have been deposited in the Electron Microscopy Data Bank [EMDB]: EB3-GTPγS MT (EMD-6347), EB3-GTPγS-K MT (EMD-6348), EB3-GTPγS-merge MT (EMD-6349, PDB: 3JAK), EB3-GMPCPP MT (EMD-6350, PDB: 3JAL), EB3-GDP MT (EMD-6351, PDB: 3JAR), GMPCPP-K MT (EMD-6352, PDB: 3JAT), GDP-K MT (EMD-6353, PDB: 3JAS) and the C1 reconstruction of EB3-consensus data (EMD-6354, PDB: 3JAW) and 13-PF GMPCPP-K MT (EMD-6355). The raw movie dataset of EB3-GDP MT is available for download at http://www.ebi.ac.uk/pdbe/emdb/empiar/ with identification number EM-PIAR-10030.

SUPPLEMENTAL INFORMATION

Supplemental Information includes Supplemental Experimental Procedures, seven figures, three tables, and four movies and can be found with this article online at http://dx.doi.org/10.1016/j.cell.2015.07.012.

AUTHOR CONTRIBUTIONS

R.Z. performed sample preparation, electron microscopy, data processing and model building/refinement. G.M.A. assisted with initial sample preparation and data collection. A.B. assisted with the model building and refinement. All authors contributed to data analysis and manuscript writing.

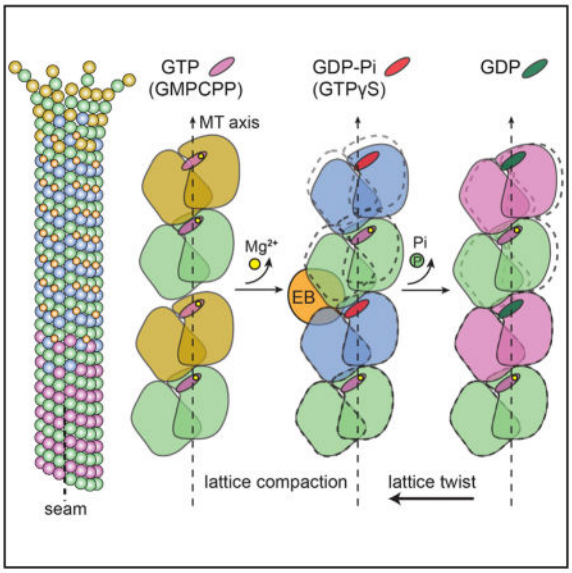

INTRODUCTION

Microtubules (MTs) are cytoskeletal polymers that play essential roles in intracellular transport, chromosome segregation, cellular organization and cell motility. They are assembled from α/β tubulin heterodimers, which stack head-to-tail into polar protofilaments, with ~13 protofilaments associating laterally in parallel to form a hollow, polar cylinder. These lateral contacts are homotypic (α-α and β-β contacts), except at a single site or "seam" (with α-β and β-α contacts) (Mandelkow et al., 1986), the functional relevance of which is not yet understood. Both in vivo and in vitro, the MT end capped by β-tubulin, termed the "plus end," undergoes stochastic switching between phases of growth and shrinkage, a hallmark behavior known as dynamic instability (Mitchison and Kirschner, 1984). This property is essential for MT function, most notably during mitosis, as highlighted by the fact that anticancer agents like Taxol inhibit cell division by stabilizing MTs and suppressing their dynamics (Dumontet and Jordan, 2010).

Dynamic instability is fundamentally linked to the nucleotide state of tubulin. α- and β-tubulin each contains a GTP binding site located at the longitudinal interface between subunits. The GTP bound at the N-site (non-exchangeable) in α-tubulin is buried at the intradimer interface where it plays a structural role (Menéndez et al., 1998), while the GTP bound at the E-site (exchangable) in β-tubulin is exposed in the unassembled dimer and is hydrolyzed within the MT via longitudinal contacts with α-tubulin as assembly proceeds (Nogales et al., 1999). A cap of GTP-tubulin (i.e., tubulin dimers containing GTP at the E-site) is thought to stabilize the plus end of the MT structure and promote its growth, while its disappearance (by GTP hydrolysis or subunit loss) makes the MT lattice unstable and prone to depolymerization (Mitchison and Kirschner, 1984).

To allow rapid remodeling of the MT cytoskeleton in response to various cellular signals, many MT-associated proteins (MAPs) are capable of modulating MT dynamics (Desai and Mitchison, 1997; Howard and Hyman, 2003). In this study, we focus on end-binding

proteins (EBs), which are the central hub for a network of plus-end tracking proteins (+TIPs) that selectively accumulate at growing MT ends (Akhmanova and Steinmetz, 2008; Galjart, 2010). EBs contain an N-terminal calponin-homology domain (CH domain) that directly interacts with the MT and mediates autonomous end-tracking (Hayashi and Ikura, 2003; Slep and Vale, 2007), a flexible linker region and a C-terminal dimerization domain that mediates recruitment of other +TIPs (Honnappa et al., 2009). Recent studies have shown that EBs also play an important role in modulating MT dynamics. Although contradictory effects have been reported, partly due to different experimental conditions (in vitro versus in vivo, different EB constructs, different affinity tags, etc.), the emerging picture is that EBs both stimulate MT growth and increase catastrophe frequency (the transition from growth to shrinkage) (Maurer et al., 2014).

Recent studies by Maurer et al. (2011) demonstrated that EB1 (and its fission yeast homolog Mal3) targets to growing MT ends by recognizing a nucleotide-dependent structural state. This state, mimicked in vitro by a GTPγS-bound MT lattice, but not the one stabilized by the slowly hydrolyzable GTP analog GMPCPP, does not exist in the body of dynamic MTs, which are composed of GDP-bound tubulin. They further reported the cryo-electron microscopy (cryo-EM) structure of Mal3-bound GTPγS MT at 8.6 Å resolution (Maurer et al., 2012), showing that Mal3 binds to four neighboring tubulins, at the junction between two protofilaments and two longitudinal interfaces.

We recently reported cryo-EM reconstructions of MTs at ~5 Å resolution, for dynamic GDP-bound and stable GMPCPP-bound MTs (Alushin et al., 2014). Comparison of these structures showed that the major change associated with GTP hydrolysis is a compaction at the interdimer interface around the E-site. At resolutions of ~5 Å, direct atomic modeling into our cryo-EM maps was not possible. Instead, we used the density map in conjunction with Rosetta modeling (Song et al., 2013) to define an ensemble of 20 low-energy structural conformers and used their average to describe each MT structure. In this study, we have now determined structures at 3.5 Å or better resolution for MTs coassembled with EB3 and EB-free MTs in different nucleotide states. Comparison of these structures has allowed us to define three nucleotide-dependent conformational states within the MT lattice, with EB proteins recognizing and promoting a hydrolysis intermediate. These findings explain both the tip-tracking behavior and the complex effect of EB proteins on MT dynamics.

RESULTS

Near-Atomic-Resolution Cryo-EM Structures of MTs in Multiple States

Using decoration with kinesin motor-domain to discriminate between α- and β-tubulin and a single particle helical reconstruction scheme implementing MT pseudo-helical symmetry, we recently reported reconstructions at 4.9 Å and 4.7 Å resolution, respectively, of dynamic GDP-bound MTs, where GTP is hydrolyzed during polymerization and stable GMPCPP-bound MTs (Alushin et al., 2014). We have now used a K2 direct electron detector (Gatan) and improved data processing strategies (see Supplemental Experimental Procedures), to obtain cryo-EM reconstructions of MTs at 3.5 Å or better resolution (Figure S1A; Table S1; Movie S1). By copolymerization with excess human EB3 (a monomeric construct lacking its C-terminal dimerization domain), we have determined the structures of EB3 bound to its

preferred substrate, GTPγS-MT (Figures 1A and 1B), as well as MTs in GMPCPP and GDP states. Our image analysis procedures allowed us to use only the small and often substoichiometric EB3 molecules as the tubulin dimer marker in the absence of kinesin. In addition, we have substantially improved the resolution of the EB-free, kinesin-decorated GMPCPP- and GDP-MTs. For completeness and comparison purposes, we obtained both a kinesin-decorated and a kinesin-free GTPγS-MT structure after coassembly with EB3. Comparison of these two structures (both at ~3.5 Å resolution) shows very similar lattice parameters (Table S2). Furthermore, merging these two datasets resulted in an improved resolution of 3.3 Å for the tubulin part (Figures 1C–1E and S1A–S1C), indicating that these two structures are practically indistinguishable and that the presence of kinesin has no significant effect on the structure of EB3-bound MTs. Interestingly, we found that kinesin competes off some of the EB3 molecules, as reflected by the weaker EB3 densities when kinesin was included (Figure S2A; Movie S1). The reconstruction shows close proximity between the α0-β1 loop of kinesin and the C-terminal end of the α6-helix of EB3 (Figure S2B), which likely results in steric clashes between these two MT binders.

GTPγS-bound tubulin is a very poor MT nucleator under the common conditions used for GTP-tubulin assembly (Hamel and Lin, 1984). Although others have described a protocol for GTPγS-tubulin assembly from GMPCPP seeds in the absence of EB3 (Maurer et al., 2011), we obtained mostly ring like structures following such protocol. Only under high glycerol concentration (~50%) were we able to form MTs with GTPγS-tubulin (or even GDP-tubulin), but such conditions are incompatible with cryo-EM imaging.

We refer to our six MT structures as EB3-GTPγS, EB3-GTPγS-K (K stands for kinesin decoration), EB3-GMPCPP, EB3-GDP, GMPCPP-K and GDP-K MTs. At a resolution of 3.4–3.5 Å, densities due to most side chains are present in these cryo-EM maps (Figure 1E), with the noticeable exception of those from acidic residues (Glu and Asp), presumably due to radiation damage during electron exposure (Allegretti et al., 2014). Although the EB3 density is at slightly lower resolution than the tubulin part (Figures S1B and S1C), it was possible to generate atomic models of both tubulin and EB3 directly from the cryo-EM maps (Table S3) and allowed the detailed visualization of EB3-tubulin interactions, the tubulin nucleotide binding pockets, the lateral contacts between protofilaments and the structure of the MT seam.

EB3-Microtubule Interactions

Our cryo-EM structure of EB3-bound GTPγS-MTs allowed us to fully visualize the interactions between the CH domain of EB3 and the four tubulin molecules it contacts (Figure 2A; Movie S2). The identified interacting residues explain well the EB mutations that abolish its end-tracking behavior (Maurer et al., 2012; Slep and Vale, 2007) (Figure S2C). On one side of EB3, two highly conserved residues, K76 and Q79, potentially hydrogen bond with the main chain of the C-terminal end of α1:H10 helix (Figure 2B), while residues L67 and H69 interact with β1:H309 and a region of the β1:T5 loop, respectively (Figure 2C). Additionally, the acid C-terminal tail (or “E-hook”) of α1-tubulin, which is unresolved beyond residue α1:E441, is located close to EB3 residues R59, K60 and potentially its basic linker region following the last resolved residue Q131 (Figure 2C),

presumably making electrostatic interactions. Such contact would be consistent with experiments showing greatly reduced affinity of MTs treated with subtilisin, which removes the C-terminal tails of tubulin, for EB1 constructs containing this linker region (Zhu et al., 2009). On the other side of EB3, our cryo-EM structure reveals the conformation of the extended N terminus of EB3 (residues 1–16) as it bridges two tubulin dimers via interactions with the α2:H4, α2:H5 and β2:H12′ helices (Figure 2D). Despite its apparent flexibility based on the relatively weaker density, the conformation of this EB3 segment is clearly different from that in the reported crystal structure (Komarova et al., 2009), indicating a reorganization upon tubulin binding. Finally, there is a major contact that involves residues R17, K100, F101 and Q102 of EB3 making extensive interactions with the β2:H3′-H3 helices (Figure 2E), with a potential cation-π interaction between EB3:R17 and β2:Y108. Interestingly, the tubulin-binding sites on the EB3 CH domain show some significant overlap with the actin-binding sites of the CH domain of fimbrin (Figure S2C) proposed in a previous cryo-EM study (Galkin et al., 2008). In contrast, the CH domain of the Ndc80 kinetochore protein, which is more divergent from EBs, interacts with completely different regions of tubulin using an alternative surface (Alushin et al., 2010).

The EB3-GTPγS-MT Has a Compacted Lattice Distinct from the Extended GMPCPP-K-MT Lattice

In our previous study, comparison of the GMPCPP-K and GDP-K MT structures showed that GTP hydrolysis results in a lattice compaction around the longitudinal interface sandwiching the E-site nucleotide (Alushin et al., 2014). This finding is now confirmed by our higher-resolution structures of these two states (Figures S3A and S3B). Unexpectedly, the EB3-GTPγS-MT structure displays a compacted lattice, making it more similar to the GDP-K state (Table S2). However, a GDP-like lattice is consistent with GTPγS-tubulin behaving like GDP-tubulin regarding its difficulty to nucleate and elongate MTs.

The lattice compaction between the GMPCPP-K and EB3-GTPγS-MT states, very similar to that seen between the GMPCPP-K and GDP-K MT structures, is best illustrated by comparing the atomic models of three longitudinally interacting tubulin dimers along a protofilament (PF) (Figures 3A and 3B), superimposing the two models on the intermediate domain of the middle β-tubulin (Figure 3A, β2-cyan). This display strategy allows the simultaneous visualization of conformational changes within the tubulin dimer (as seen in the central β2-α2 dimer), as well as the associated compaction along the protofilament (illustrated by the up and down movement, respectively, of the top and bottom dimers). Cα-RMSD analysis (Figure 3B; Movie S3) clearly shows a lack of significant domain rearrangement within β-tubulin, with only small, local changes around the E-site, as can be best seen in β2-tubulin. On the other hand, there is a significant displacement of the dimer above (β3-α3) and below (β1-α1), compacting the E-sites, that is coupled to a notable rearrangement of α-tubulin, as can be best seen in α2-tubulin. Interestingly, there is an “anchor point” across the longitudinal interface, contacting the E-site and near the MT surface, that does not move (Figure 3B, red arrow, Figure 3C, red circle). This unaffected contact involves hydrophobic interactions between the H8 helix and S7-H8 loop of α-tubulin and the H11′ helix of β-tubulin (Figure 3D). Thus, the compaction brings every two adjacent dimers along the protofilament closer to each other around an anchor point between

them, necessarily resulting in a conformational rearrangement of every α-tubulin. Within α-tubulin, the intermediate domain and the C-terminal H11-H12 helices undergo a small rotation with respect to the N-terminal nucleotide-binding domain (Figure S4A, black arrow), which maintains its relative position with respect to the β-tubulin within the same dimer (Figure 3B, see both α3- and α2-tubulin). The H8 helix and S7-H8 loop display the largest changes, which appear to be coupled to the movement of the next tubulin dimer (Figure 3B, red and cyan arrows).

The atomic models derived from our high-resolution reconstructions allow us to describe in detail the subtle changes around the E-site nucleotide that ultimately result in the observed lattice compaction. The α:H8 helix, which bridges the anchor point and α:T7 loop, an element that contacts the E-site nucleotide and that moves during the compaction, is noticeably distorted at its N-terminal end (residues 251–254) in the EB3-GTPγS (and GDP-K) state (Figure 3C, red arrow). Importantly, this distorted region contains the proposed catalytic residue α:E254. Additionally, the β:T2-H2 region (residues 71–76) has moved closer to the nucleotide in the EB3-GTPγS (andGDP-K) state(Figure 3E, red arrow), a change that resembles that seen when comparing X-ray crystal structures of β-tubulin bound to GTP (or GMPCPP) and GDP (Nawrotek et al., 2011) (Figure S4C). This change may be caused by the loss of the neighboring Mg^{2+} ion accompanying GTP hydrolysis (see Discussion). We also observe significant movement of the β:T5 loop, especially for residues 175–177 (Figure 3E), that is coupled to the downward movement of the S9 β strand and H10 helix of α-tubulin across the interdimer interface (Figure 3E). A further change occurs away from the E-site (Figure 3B, black arrow), involving the C-terminal end of the α:H5 helix (residues 189–198), a site in α-tubulin that needs to accommodate the relative movement between the α:H4 helix and the α:H8-S7 loop during lattice compaction (Figure 3F, red circle). Interestingly, these regions of nucleotide-dependent changes in β:T5 and α:H5 constitute major contact points with EB3 (Figures 2C and 2D) and thus contribute to the MT nucleotide state discrimination of EB3.

EB3-GTPγS-MT and GDP-K-MT Have Different Lattice Twist

Comparison of the atomic models of the two compacted states (EB3-GTPγS and EB-free GDP-K MTs) shows a small but noticeable relative rotation between adjacent tubulin dimers along a PF, that can be best visualized when comparing three consecutive dimers of both states, aligning on the β subunit of the bottom dimer (Figures 4A and 4B). This “dimer-rotation” is in a direction tangential to the MT surface and perpendicular to the MT axis (Figures S3C, S5A, and S5B). Interestingly, it maintains the same anchor point at the intradimer interface (Figure 4F, red circle). Since no compensatory domain rotation occurs within α- or β-tubulin (Figure 4B), this relative dimer-rotation causes the PF to run at a slightly different tilt angle (Figures 4A, S5A, and S5B). This intrinsic tilt of a PF necessarily leads to a global “lattice twist” in the 3D reconstruction. The amount of lattice twist can be directly measured from the cryo-EM density map in terms of “dimer-twist” (Table S2), a helical symmetry parameter that defines the amount of rotation around the MT axis and that, combined with the necessary vertical shift, aligns one tubulin dimer to the next dimer along the PF (Figure 1A, black dashed line). Further analysis indicates that this intrinsic tilt of a

PF (revealed by directly aligning the atomic models) is only related to the nucleotide states (and EB3-binding to some extent) but not the PF numbers (Figures S5C–S5F).

In contrast to the significant local changes around the E-site upon lattice compaction, including α:H8, β:T2-H2 and β:T5, we observe minimal changes of the backbone geometry of these key structural elements between the two compacted states (EB3-GTPγS and GDP-K) (Figure 4F). However, the relative dimer-rotation across the E-site between these two states causes a noticeable shift of the α:T7 loop and the N-terminal end of α:H8 with respect to the unchanging anchor point and the E-site nucleotide (Figure 4F, red arrow). Additionally, root-mean-square deviation (RMSD) analysis reveals three clear changes distal from the E-site (Figure 4B, red and cyan arrows): at the M-loops of both α- and β-tubulin (Figures 4C and 4D, red circles), which are most likely due to different PF numbers; and at the C-terminal end of α:H10 helix (residues 337–342) (Figure 4E, cyan circle), a major contact point for EB3 (Figure 2B) that may be altered as a result of EB3 binding and/or serve as a discriminating factor for EB3 affinity.

Comparing all of our structures, we do not detect any significant movement of the β:T3 loop or the following H3′-H3 helices (Figures 3E and 4F), which have been proposed to undergo a nucleotide-dependent change that could be detected by EBs (Maurer et al., 2012). In fact, the conformation of β:T3 and β:H3′-H3 in all our EM structures is also very similar to that in high-resolution crystal structures of unassembled tubulin, regardless of the nucleotide state (Nawrotek et al., 2011; Prota et al., 2013) (Figure S4D).

EB Promotes a Specific MT Lattice during Polymerization and Increases the Rate of GTP Hydrolysis

Based on the changes described above, binding of EB3 across four tubulin dimers on the MT lattice presumably makes this protein exquisitely sensitive to the lattice rearrangement that accompanies GTP hydrolysis. Comparisons of the EB-binding pocket in the EB3-GTPγS-MT structure with the equivalent regions in the 13-PF EB3-free GDP-K and GMPCPP-K-MT lattice show noticeable differences (Figures 4G and 4H), explaining the different affinities of EB3 for MTs in different nucleotide states. The differences are even larger if comparing the 13-PF EB3-GTPγS-MT with the 14-PF GMPCPP-K and GDP-K-MT structures (Figures S5G and S5H). Additionally, nucleotide-dependent conformational changes at individual EB3:tubulin contact points, such as those seen for β:T5 (Figure 3E), α:H5 (Figure 3F) and α:H10 (Figure 4E), may also contribute to the discrimination among nucleotide states.

To further analyze the lattice preference of EB3 and its effect on MT dynamics, we also determined the structures of EB3-decorated GMPCPP- and GDP-MTs by copolymerization with excess EB3. Under such assembly conditions, the MT population shifts to almost 100% 13-PFs (Table S1), consistent with previous studies (des Georges et al., 2008; Maurer et al., 2012; Vitre et al., 2008). Furthermore, the lattice parameters of both the EB3-GMPCPP and EB3-GDP MTs shift toward that of the EB3-GTPγS state (Table S2). Thus, coassembly with EB3 affects the MT lattice and suppresses the differences normally caused by nucleotide state. The resolution of our structures (3.5 Å or better) allowed us to directly assess the presence of the γ-phosphate and/or the Mg^{2+} ion for the different MT states (Figure 5). In all

cases, the N-site displays clear densities for both the γ-phosphate and the Mg^{2+} ion. Concerning the E-site, only the GMPCPP-K-MT structure shows both the γ-phosphate and Mg^{2+}, while both elements are missing in the GDP-K-MT and EB3-GDP-MT states, as expected from hydrolysis of GTP during assembly. Importantly, in the EB3-GTPγS-MT structure, the density corresponding to the γ-phosphate is clearly visible, while the Mg^{2+} ion is not present (Figure 5, red arrows). Most interestingly, in the EB3-GMPCPP-MT structure, both the Mg^{2+} and the γ-phosphate are missing from the E-site (Figure 5, black arrow). It is important to emphasize that the EB-free and EB3-coassembled GMPCPP-MT reconstructions were obtained from MT samples prepared back-to-back, using the same GMPCPP-bound tubulin samples and a final buffer free of sodium ions (known to speed up the hydrolysis of GMPCPP) (Caplow et al., 1994). Our results indicate that EB3 quickly stimulates hydrolysis, within two minutes of MT assembly, of this otherwise slowly hydrolyzable GTP analog, explaining the lattice compaction we observe. We speculate that by binding across four tubulin dimers, EB3 promotes a compacted MT lattice that facilitates access of the catalytic residue E254 in the α:H8 helix to the E-site nucleotide. Thus, the distributed interactions of EB3 across tubulin subunits make it not only sensitive to the lattice rearrangements that accompany GTP hydrolysis, but also capable itself of modulating the lattice to promote a structural state that increases the hydrolysis rate.

Despite the overall similarities between the three EB3-bound MT structures, we quantitatively estimated the EB3 occupancy (see Supplemental Experimental Procedures) of the GTPγS-MT to be significantly higher than the other two nucleotide states (Table S2), which is also apparent from the cryo-EM densities (Figures S6G–S6I; Movie S1). This result is in agreement with the proposal that GTPγS-MT is the preferred MT substrate for EBs binding (Maurer et al., 2011). Interestingly, the reconstructions from the EB3-GDP-MT and EB3-GMPCPP-MT samples, both of which are missing the γ-phosphate and Mg^{2+} ion at the E-site (Figure 5) and thus are ultimately both in a GDP state, have a similar dimer-twist (−0.1°) that is halfway between the EB3-GTPγS-MT (−0.3°), which is the state of high EB3 affinity and the 13-PF EB-free GDP-K-MT (0°), which has much lower affinity for EBs. The correlation between the degree of lattice twist and EB3-occupancy (Table S2) strongly suggests that EB is sensitive to the subtle changes in lattice twist. It also supports the idea that EB promotes a lattice twist that optimizes its own binding site.

Lateral Interface between Protofilaments and at the MT Seam

The resolution of our structures allows us to reveal the atomic details of the native lateral contacts between protofilaments (Figure 6A; Movie S4), which were poorly defined in our previous study (Rosetta ensembles had poor convergence at the lateral interface) (Alushin et al., 2014). All our structures show very similar lateral contacts, irrespective of nucleotide state, with small changes seen only for MTs with different PF numbers (Figures 4C and 4D). In all cases, the lateral interface is limited to a single point of contact that involves the M-loop (S7-H9 loop) on one side, sandwiched on the other side by the H2-S3 loop and a β-hairpin structure in the H1′-S2 loop (Figures 6B and 6C), with exquisite shape complementarity that resembles a lock-and-key configuration. Within the MT lattice, the M-loop of both α- and β-tubulin adopts a helical conformation, positioning a strategic aromatic residue on the M-loop, H283 in α-tubulin and Y283 in β-tubulin, to function as a “key” that

inserts into a complementary “lock” formed by the H2-S3 and H1′-S2 loops (Figures 6B and 6C). Additionally, residue K60 in the H1′-S2 loop, conserved between α- and β-tubulin, appears to be fully extended and further “locking” the position of the aromatic residue Y/H283. In contrast to a previous report based on a lower resolution cryo-EM structure of Mal3-GTPγS-MT (Maurer et al., 2012), we do not observe additional lateral contacts involving β:H3 and the neighboring β:H9 helices in our EB3-GTPγS-MT structure.

The use of a direct electron detector and our improved accuracy in determining the seam location allowed us to obtain asymmetric (C1) reconstructions at 4.4 Å or better resolution for all MT states, with the exception of the 13-PF GDP-K-MT due to the limited number of MT segments (Table S1). All the C1 reconstructions show B-lattices with a single seam. Those with EB3-bound clearly show that EB3 does not bind to the MT seam (Figures 1B, 6G, and S6G–S6I), as previously observed (Maurer et al., 2012). Our result contrasts with a previous study where high concentration of Mal3 gave rise to a high percentage of A-lattice content (des Georges et al., 2008). This discrepancy may be due to the source of tubulin, which was His-tag *S. pombe* tubulin rather than the untagged porcine used here.

When we superimposed the atomic models fitted into the C1 and symmetrized reconstructions of the EB-free MT structures, the relative positions of PFs show very good agreement, with the exception of the two PFs across the seam, which are further apart from each other in the C1 reconstruction (Figures 6G and S6A–S6C). In comparison, all the EB3-bound MT states show minimal differences between the C1 and symmetrized reconstructions (Figures 6H and S6D–S6F), suggesting that EB3 binding regularizes the MT lattice, making it more symmetric and presumably more stable. This is consistent with the fact that to reach the same resolution, substantially fewer particles were needed for any of the EB3-bound MT states than for the EB-free MT states (Table S1). It is also noteworthy that in the 13-PF GMPCPP-K-MT, which is more rare, the two PFs at the seam are further apart than those of the more stable 14-PF counterpart.

It has previously been reported that EBs promote MT sheet closure in vitro (Vitre et al., 2008). Consistently, in our raw cryo-EM images of MTs copolymerized with EB3, we rarely observe open sheet structures at the end of fast growing MTs (within 1–2 min of the start of polymerization). In comparison, in the absence of EB, we often observe large sheet-like structures at growing ends of dynamic MTs (Figure S7). The effect of sheet-closure by EB may seem counterintuitive, considering the fact that EB does not bind to the MT seam. However, our finding that EB binding regularizes the lattice suggests that by binding between adjacent PFs and imposing a specific curvature, EB would consequently promote sheet closure by bringing the two PFs across the seam closer, thus presumably strengthening the lateral interaction at the seam. In the absence of EB, the greater distance between PFs at the seam likely results in weaker lateral contacts.

Despite the subtle differences in lattice twist for the three EB3-bound states, their structures are similar enough to allow us to merge the datasets and obtain a C1 reconstruction of an “EB-consensus” map at an improved resolution (3.9 Å around the seam). This resolution allowed us to analyze the lateral interactions at the seam at the side-chain level (Figure 6D). The seam contact is similar to that seen at a non-seam location (Figures 6E and 6F), as

previously suggested (Sui and Downing, 2010), likely due to the high degree of conservation of the residues involved in the lateral contacts between α- and β-tubulin. However, due to differences in the position of the H2-S3 loop between α- and β-tubulin (Figures 6E and 6F, dashed arrows), small adjustments are needed to optimize contacts while avoiding steric clashes between adjacent PF at the seam.

DISCUSSION

Tubulin Changes Conformation around an Anchor Point at the Interdimer Longitudinal Interface

The studies presented here define the conformational landscape for tubulin within the MT lattice and its relationship to the process of dynamic instability and its regulation by EB proteins. The two global MT lattice rearrangements described here, i.e., the lattice compaction between the GMPCPP-K-MT and EB3-GTPγS-MT/GDP-K-MT and the lattice twist between the EB3-GTPγS-MT and the GDP-K-MT, both involve the movement of α-tubulin around an anchor point at the interdimer longitudinal interface (Figures 3C and 4D). Interestingly, this anchor point appears to be extremely robust and is maintained in all published tubulin structures that involve interactions between dimers, including all the crystal structures of tubulin bound to RB3 (a stathmin homolog that sequesters two dimers) (Figure S4D). The crystal structures correspond to a “bent” tubulin state that is believed to approximate the depolymerized state of tubulin as observed in protofilament peels of disassembling MTs. Based on this idea and the fact that the anchor point is located at the outer surface of the MT, MT depolymerization likely involves a relative rotation between tubulin dimers (or monomers) around this anchor point, which would remain as an unchanged interaction within protofilament peels.

Link between GTP Analog-Bound MT Structures and GTP Hydrolysis

In our efforts to approximate the structural states of tubulin within the MT before and after GTP hydrolysis, we have made use of two different GTP analogs: GMPCPP and GTPγS. A precise measurement of the distance between α- and β-tubulin across the E-site and N-site (we refer to these as the interdimer and intradimer subunit distance, respectively) show that among different MT states, all the intradimer distances are very similar (41.5 ± 0.1 Å), while the interdimer distances fall into two groups, corresponding to extended and compacted lattice states (Table S2). Notably, the GMPCPP-K-MT has an interdimer distance that is very close to the intradimer distance, suggesting that GMPCPP bound at the E-site is equivalent to GTP bound at the N-site. These structural results, together with the fact that GMPCPP-tubulin readily nucleates and elongates MTs (Hyman et al., 1992), a behavior similar to GTP-tubulin, strongly indicate that the GMPCPP-MT state is a good approximation of the GTP-MT state. Therefore, it is reasonable to think of the GMPCPP-MT state as a surrogate for the GTP-cap at the growing end of dynamic MTs.

On the other hand, GTPγS-tubulin behaves similarly to GDP-tubulin, in that it cannot nucleate or readily elongate MTs. Our studies now show that structurally the GTPγS-MT state also resembles the GDP-MT state in terms of a compacted lattice and very similar tubulin structures at the monomer level. Most importantly, both structures are missing the

Mg^{2+} ion at the E-site (Figure 5). In the presence of EB proteins and GMPCPP-MT seeds, however, GTPγS-tubulin readily incorporates into the MT, with a unique lattice twist and displays higher affinity for EB3 than the GMPCPP-MT (mimicking the GTP-cap) or the GDP-MT (corresponding to the body of dynamic MTs where hydrolysis has taken place). Although copolymerization with excess of EB3 enforces a specific MT lattice and largely overrides the structural effects of nucleotide state, the stronger EB3 densities for the GTPγS-MT than the other two nucleotide states suggests that the GTPγS state is a mimic of a naturally occurring intermediate state during GTP hydrolysis that EBs recognize and preferentially bind. Interestingly, it has been recently found that the comet-like density profiles of GFP-EB1 lag several tens of nanometers behind the extreme MT plus-end, where the tubulin is presumably in the GTP state (Maurer et al., 2014). All these structural and biochemical evidence leads us to propose that GTPγS may mimic a post-hydrolysis state, probably a GDP-Pi state that precedes the release of the inorganic phosphate.

GTP Hydrolysis Generates Conformational Strain in the MT Lattice

Our high-resolution cryo-EM structures reveal that the N-terminal end of α:H8 helix (residues D251 to E254) is noticeably distorted from an ideal α-helix in both the EB3-GTPγS and GDP-K states, but not in the GMPCPP-K state (Figures 3C, S4E, and S4F), suggesting this conformational transition is directly caused by GTP hydrolysis and/or the loss of the coordinating Mg^{2+} ion. Notably, residue α:E254 is believed to be the catalytic residue in polymerization-dependent GTP hydrolysis (Anders and Botstein, 2001; Nogales et al., 1998a, 1998b; Oliva et al., 2004). Interestingly, the “undistorted” conformation of α:H8 in the GMPCPP-K state not only resembles that of the β:H8 in all of our EM structures (Figure S4E), but also resembles the conformation of both α:H8 and β:H8 in all the available crystal structures, regardless of nucleotide state (Figure S4F). In such structures residue α:E254 is located far away from the γ-phosphate in the adjacent β-tubulin, thus preventing GTP hydrolysis out of the lattice context.

Given that a distorted conformation of α:H8 is only found in the GTPγS and GDP states within the MT (both are post-hydrolysis states and missing the Mg^{2+} ion at the E-site), but not in the GMPCPP state (a pre-hydrolysis state) or in the crystal structures, where tubulin is free of lattice constraints, our structural results suggests that the α:H8 distortion contributes to the mechanical strain on the MT lattice hypothesized to follow GTP hydrolysis (Caplow et al., 1994). Another conformational change following hydrolysis that likely contributes to lattice strain concerns the relative rotation of the intermediate domain and C-terminal helices of α-tubulin with respect to its N-terminal domain (Figure S4A). Interestingly, as the lattice compacts, the rotation is away from that observed in the proposed “ground state” represented by the crystal structures (Rice et al., 2008) (Figure S4B), further supporting the idea that GTP hydrolysis generates mechanical strain.

EB Promotes Structural Transitions at the Plus Ends of Growing MTs

Our cryo-EM structures of MTs coassembled with EB3 show that the presence of EB promotes a compacted MT lattice with a unique lattice twist, which EB itself preferentially binds. This state is compacted across the E-site, yet distinct from the EB-free GDP-K state in terms of lattice twist. We propose this state mimics an intermediate state in the GTP

hydrolysis cycle, best represented by the GTPγS state. Additionally, this specific MT lattice also stimulates the rapid hydrolysis of GMPCPP. A previous study by Maurer et al. (2014) suggested that growing MT ends mature in at least two distinct kinetic steps, with EB proteins accelerating both structural transitions. In light of our high-resolution structures, EB may catalyze the first structural transition by strengthening lateral and longitudinal interactions between dimers and promoting a compacted MT lattice. Given that EB proteins have distributed interactions across four neighboring tubulin subunits, EB binding to the MT may occur in multiple steps that engage progressively more of these contacts, with MT lattice compaction happening with full EB engagement. The compacted lattice could then speed up GTP hydrolysis, presumably by positioning the catalytic residue E254 in α-tubulin closer to the E-site nucleotide (Figures S3D and S3E). Interestingly, it has been observed that higher concentrations of GFP-EB1 produces shorter comet-like density profiles of EB1 at growing MT ends and shift their peaks closer to the extreme MT ends (Maurer et al., 2014). The second structural transition, i.e., the change in lattice twist, may naturally occur between the GDP-Pi state and the final GDP state upon phosphate release, with the more twisted (Table S2, in the context of 13-PF MTs) and short-lived GDP-Pi state being recognized by fully engaged EB proteins. Alternatively, the full EB binding may itself induce a “twisted” MT lattice, which may only be optimally accommodated by the MT in a GDP-Pi state (and best mimicked by GTPγS state), perhaps by having a unique protofilament bending or tilting capability (Figure 4A). Such lattice twist would be transient, as the subsequent phosphate release results in a GDP-MT lattice, which we observe to be less twisted, even in the presence of excess EB3 (Table S2). While our structural data cannot discriminate between these two models, we favor the second, which is more in line with the previously proposed “structural plasticity” model for MT dynamics (Kueh and Mitchison, 2009).

In conclusion, our structural results, combined with previous biochemical data, depict an emerging picture of the detailed mechanism of the GTP hydrolysis-coupled transitions within the MT lattice that govern MT dynamic instability and their modulation by EB proteins. Based on our model (Figure 7), hydrolysis from GTP to GDP-Pi is coupled to a large conformational change, i.e., lattice compaction, as well as local rearrangements around the E-site nucleotide (in α:T7-H8, β:T2-H2 and β:T5). During this process α:E254 is repositioned for catalysis and Mg^{2+} is likely released. The second step, phosphate release, results in a final GDP state in the body of the MT. While lateral contacts are not significantly affected by nucleotide state, the strain generated in the tubulin subunit following GTP hydrolysis described here, will promote the breakage of lateral contacts, likely initiated at the weaker seam interface. EBs promote MT growth by binding at the intersection of lateral and longitudinal contacts and enforcing the proper geometry of contacts to facilitate seam closure. On the other hand, EBs preferentially bind to and/or facilitate the transient intermediate GDP-Pi state, promoting lattice compaction and GTP hydrolysis, then lose their affinity for the MT lattice upon the subsequent phosphate release.

EXPERIMENTAL PROCEDURES

Full details of the experimental procedures are presented in the Supplemental Experimental Procedures.

Sample Preparation for Cryo-EM

The kinesin decorated GMPCPP-MT and dynamic GDP-MT were prepared as previously described (Alushin et al., 2014) (see Supplemental Experimental Procedures for details). The GTPγS-MT were grown out of short GMPCPP-MT seeds in the presence of excess EB3, similar to a previous protocol (Maurer et al., 2011). The MTs were polymerized directly on a glow-discharged C-flat holey carbon grid (Protochips) inside a Vitrobot (FEI) set at 37°C and 95% humidity, for 2 min before plunge-freezing in ethane slush. The EB3-decorated GMPCPP-MTs were obtained in a similar way, but without the GMPCPP-MT seeds. Since GTP-tubulin is less efficiency in nucleating MTs than GMPCPP-tubulin, the EB3-decorated GDP-MTs were prepared outside the Vitrobot at 37°C, without the MT seeds, for ~15 min before plunge freezing.

Cryo-Electron Microscopy

Imaging was performed using a Titan microscope (FEI) operated at an accelerating voltage of 300 kV. All cryo-EM images were recorded on a K2 Summit direct electron detector (Gatan), at a nominal magnification of 27,500 ×, corresponding to a calibrated pixel size of 1.32 Å. The camera was operated in counting mode, with a dose rate of ~8 electrons/pixel/s on the detector camera. A total exposure time of 6 s, corresponding to a total dose of 27.6 electrons/$Å^2$ on the specimen, was fractionated into 20 movie frames. The data were collected semi-automatically using the Leginon software suite (Suloway et al., 2005).

Image Processing

The image processing pipeline resembled that previously described (Alushin et al., 2014), with modifications (see Supplemental Experimental Procedures). In addition to the drift-correction performed on the entire micrograph using the UCSF *motioncorr* program (Li et al., 2013), the recorded movie frames allowed us to track the independent movement of each MT within the same micrograph (Campbell et al., 2012), resulting in a resolution improvement.

Atomic Model Building and Refinement

Our high-resolution cryo-EM density maps allowed us to use COOT (Emsley et al., 2010) to directly build the entire polypeptide chains of α/β tubulin and EB3, using available crystal structures as starting models. The models built in COOT were subsequently refined with REFMAC v5.8 optimized for refinement into EM maps (Brown et al., 2015), following a previous protocol (Amunts et al., 2014).

Supplementary Material

Refer to Web version on PubMed Central for supplementary material.

Acknowledgments

We are grateful to Robert Glaeser for the use of the Titan microscope and for stimulating discussions. We thank Anchi Cheng and Tom Houwelling for assistance with Leginon installation and APPION data processing. We thank Alexis Rohou and Nikolaus Grigorieff for guidance in the use of FREALIGN. We also thank Stuart Howes for the purification of kinesin. The kinesin expression construct was a gift from Erik Jonsson and Ron, and the EB3 cDNA

was a gift from Clare Waterman. This work was funded by a grant from the NIGMS (GM051487 to E.N.). E.N. is a Howard Hughes Medical Institute investigator.

References

Akhmanova A, Steinmetz MO. Tracking the ends: a dynamic protein network controls the fate of microtubule tips. Nat Rev Mol Cell Biol. 2008; 9:309–322. [PubMed: 18322465]

Allegretti M, Mills DJ, McMullan G, Kühlbrandt W, Vonck J. Atomic model of the F420-reducing [NiFe] hydrogenase by electron cryo-microscopy using a direct electron detector. eLife. 2014; 3:e01963. [PubMed: 24569482]

Alushin GM, Ramey VH, Pasqualato S, Ball DA, Grigorieff N, Musacchio A, Nogales E. The Ndc80 kinetochore complex forms oligomeric arrays along microtubules. Nature. 2010; 467:805–810. [PubMed: 20944740]

Alushin GM, Lander GC, Kellogg EH, Zhang R, Baker D, Nogales E. High-resolution microtubule structures reveal the structural transitions in αβ-tubulin upon GTP hydrolysis. Cell. 2014; 157:1117–1129. [PubMed: 24855948]

Amunts A, Brown A, Bai XC, Llácer JL, Hussain T, Emsley P, Long F, Murshudov G, Scheres SH, Ramakrishnan V. Structure of the yeast mitochondrial large ribosomal subunit. Science. 2014; 343:1485–1489. [PubMed: 24675956]

Anders KR, Botstein D. Dominant-lethal alpha-tubulin mutants defective in microtubule depolymerization in yeast. Mol Biol Cell. 2001; 12:3973–3986. [PubMed: 11739794]

Brown A, Long F, Nicholls RA, Toots J, Emsley P, Murshudov G. Tools for macromolecular model building and refinement into electron cryo-microscopy reconstructions. Acta Crystallogr D Biol Crystallogr. 2015; 71:136–153. [PubMed: 25615868]

Campbell MG, Cheng A, Brilot AF, Moeller A, Lyumkis D, Veesler D, Pan J, Harrison SC, Potter CS, Carragher B, Grigorieff N. Movies of ice-embedded particles enhance resolution in electron cryo-microscopy. Structure. 2012; 20:1823–1828. [PubMed: 23022349]

Caplow M, Ruhlen RL, Shanks J. The free energy for hydrolysis of a microtubule-bound nucleotide triphosphate is near zero: all of the free energy for hydrolysis is stored in the microtubule lattice. J Cell Biol. 1994; 127:779–788. [PubMed: 7962059]

des Georges A, Katsuki M, Drummond DR, Osei M, Cross RA, Amos LA. Mal3, the Schizosaccharomyces pombe homolog of EB1, changes the microtubule lattice. Nat Struct Mol Biol. 2008; 15:1102–1108. [PubMed: 18794845]

Desai A, Mitchison TJ. Microtubule polymerization dynamics. Annu Rev Cell Dev Biol. 1997; 13:83–117. [PubMed: 9442869]

Dumontet C, Jordan MA. Microtubule-binding agents: a dynamic field of cancer therapeutics. Nat Rev Drug Discov. 2010; 9:790–803. [PubMed: 20885410]

Emsley P, Lohkamp B, Scott WG, Cowtan K. Features and development of Coot. Acta Crystallogr D Biol Crystallogr. 2010; 66:486–501. [PubMed: 20383002]

Galjart N. Plus-end-tracking proteins and their interactions at microtubule ends. Curr Biol. 2010; 20:R528–R537. [PubMed: 20620909]

Galkin VE, Orlova A, Cherepanova O, Lebart MC, Egelman EH. High-resolution cryo-EM structure of the F-actin-fimbrin/plastin ABD2 complex. Proc Natl Acad Sci USA. 2008; 105:1494–1498. [PubMed: 18234857]

Hamel E, Lin CM. Guanosine 5′-O-(3-thiotriphosphate), a potent nucleotide inhibitor of microtubule assembly. J Biol Chem. 1984; 259:11060–11069. [PubMed: 6381495]

Hayashi I, Ikura M. Crystal structure of the amino-terminal microtubule-binding domain of end-binding protein 1 (EB1). J Biol Chem. 2003; 278:36430–36434. [PubMed: 12857735]

Honnappa S, Gouveia SM, Weisbrich A, Damberger FF, Bhavesh NS, Jawhari H, Grigoriev I, van Rijssel FJ, Buey RM, Lawera A, et al. An EB1-binding motif acts as a microtubule tip localization signal. Cell. 2009; 138:366–376. [PubMed: 19632184]

Howard J, Hyman AA. Dynamics and mechanics of the microtubule plus end. Nature. 2003; 422:753–758. [PubMed: 12700769]

Hyman AA, Salser S, Drechsel DN, Unwin N, Mitchison TJ. Role of GTP hydrolysis in microtubule dynamics: information from a slowly hydrolyzable analogue, GMPCPP. Mol Biol Cell. 1992; 3:1155–1167. [PubMed: 1421572]

Komarova Y, De Groot CO, Grigoriev I, Gouveia SM, Munteanu EL, Schober JM, Honnappa S, Buey RM, Hoogenraad CC, Dogterom M, et al. Mammalian end binding proteins control persistent microtubule growth. J Cell Biol. 2009; 184:691–706. [PubMed: 19255245]

Kueh HY, Mitchison TJ. Structural plasticity in actin and tubulin polymer dynamics. Science. 2009; 325:960–963. [PubMed: 19696342]

Li X, Mooney P, Zheng S, Booth CR, Braunfeld MB, Gubbens S, Agard DA, Cheng Y. Electron counting and beam-induced motion correction enable near-atomic-resolution single-particle cryo-EM. Nat Methods. 2013; 10:584–590. [PubMed: 23644547]

Mandelkow EM, Schultheiss R, Rapp R, Müller M, Mandelkow E. On the surface lattice of microtubules: helix starts, protofilament number, seam and handedness. J Cell Biol. 1986; 102:1067–1073. [PubMed: 3949873]

Maurer SP, Bieling P, Cope J, Hoenger A, Surrey T. GTPgammaS microtubules mimic the growing microtubule end structure recognized by end-binding proteins (EBs). Proc Natl Acad Sci USA. 2011; 108:3988–3993. [PubMed: 21368119]

Maurer SP, Fourniol FJ, Bohner G, Moores CA, Surrey T. EBs recognize a nucleotide-dependent structural cap at growing microtubule ends. Cell. 2012; 149:371–382. [PubMed: 22500803]

Maurer SP, Cade NI, Bohner G, Gustafsson N, Boutant E, Surrey T. EB1 accelerates two conformational transitions important for microtubule maturation and dynamics. Curr Biol. 2014; 24:372–384. [PubMed: 24508171]

Menéndez M, Rivas G, Díaz JF, Andreu JM. Control of the structural stability of the tubulin dimer by one high affinity bound magnesium ion at nucleotide N-site. J Biol Chem. 1998; 273:167–176. [PubMed: 9417061]

Mitchison T, Kirschner M. Dynamic instability of microtubule growth. Nature. 1984; 312:237–242. [PubMed: 6504138]

Nawrotek A, Knossow M, Gigant B. The determinants that govern microtubule assembly from the atomic structure of GTP-tubulin. J Mol Biol. 2011; 412:35–42. [PubMed: 21787788]

Nogales E, Downing KH, Amos LA, Löwe J. Tubulin and FtsZ form a distinct family of GTPases. Nat Struct Biol. 1998a; 5:451–458. [PubMed: 9628483]

Nogales E, Wolf SG, Downing KH. Structure of the alpha beta tubulin dimer by electron crystallography. Nature. 1998b; 391:199–203. [PubMed: 9428769]

Nogales E, Whittaker M, Milligan RA, Downing KH. High-resolution model of the microtubule. Cell. 1999; 96:79–88. [PubMed: 9989499]

Oliva MA, Cordell SC, Löwe J. Structural insights into FtsZ protofilament formation. Nat Struct Mol Biol. 2004; 11:1243–1250. [PubMed: 15558053]

Prota AE, Bargsten K, Zurwerra D, Field JJ, Díaz JF, Altmann KH, Steinmetz MO. Molecular mechanism of action of microtubule-stabilizing anticancer agents. Science. 2013; 339:587–590. [PubMed: 23287720]

Rice LM, Montabana EA, Agard DA. The lattice as allosteric effector: structural studies of alphabeta- and gamma-tubulin clarify the role of GTP in microtubule assembly. Proc Natl Acad Sci USA. 2008; 105:5378–5383. [PubMed: 18388201]

Slep KC, Vale RD. Structural basis of microtubule plus end tracking by XMAP215, CLIP-170 and EB1. Mol Cell. 2007; 27:976–991. [PubMed: 17889670]

Song Y, DiMaio F, Wang RY, Kim D, Miles C, Brunette T, Thompson J, Baker D. High-resolution comparative modeling with Roset-taCM. Structure. 2013; 21:1735–1742. [PubMed: 24035711]

Sui H, Downing KH. Structural basis of interprotofilament interaction and lateral deformation of microtubules. Structure. 2010; 18:1022–1031. [PubMed: 20696402]

Suloway C, Pulokas J, Fellmann D, Cheng A, Guerra F, Quispe J, Stagg S, Potter CS, Carragher B. Automated molecular microscopy: the new Leginon system. J Struct Biol. 2005; 151:41–60. [PubMed: 15890530]

Vitre B, Coquelle FM, Heichette C, Garnier C, Chrétien D, Arnal I. EB1 regulates microtubule dynamics and tubulin sheet closure in vitro. Nat Cell Biol. 2008; 10:415–421. [PubMed: 18364701]

Zhu ZC, Gupta KK, Slabbekoorn AR, Paulson BA, Folker ES, Goodson HV. Interactions between EB1 and microtubules: dramatic effect of affinity tags and evidence for cooperative behavior. J Biol Chem. 2009; 284:32651–32661. [PubMed: 19778897]

Highlights

- 3.5 Å microtubule structures in different nucleotide states, with and without EB3
- Changes in α-tubulin with GTP hydrolysis generate strain in the lattice
- The EB3-bound GTPγS-microtubule is compacted with a unique twist
- EB3 binding promotes lattice compaction, GTP hydrolysis and seam closure

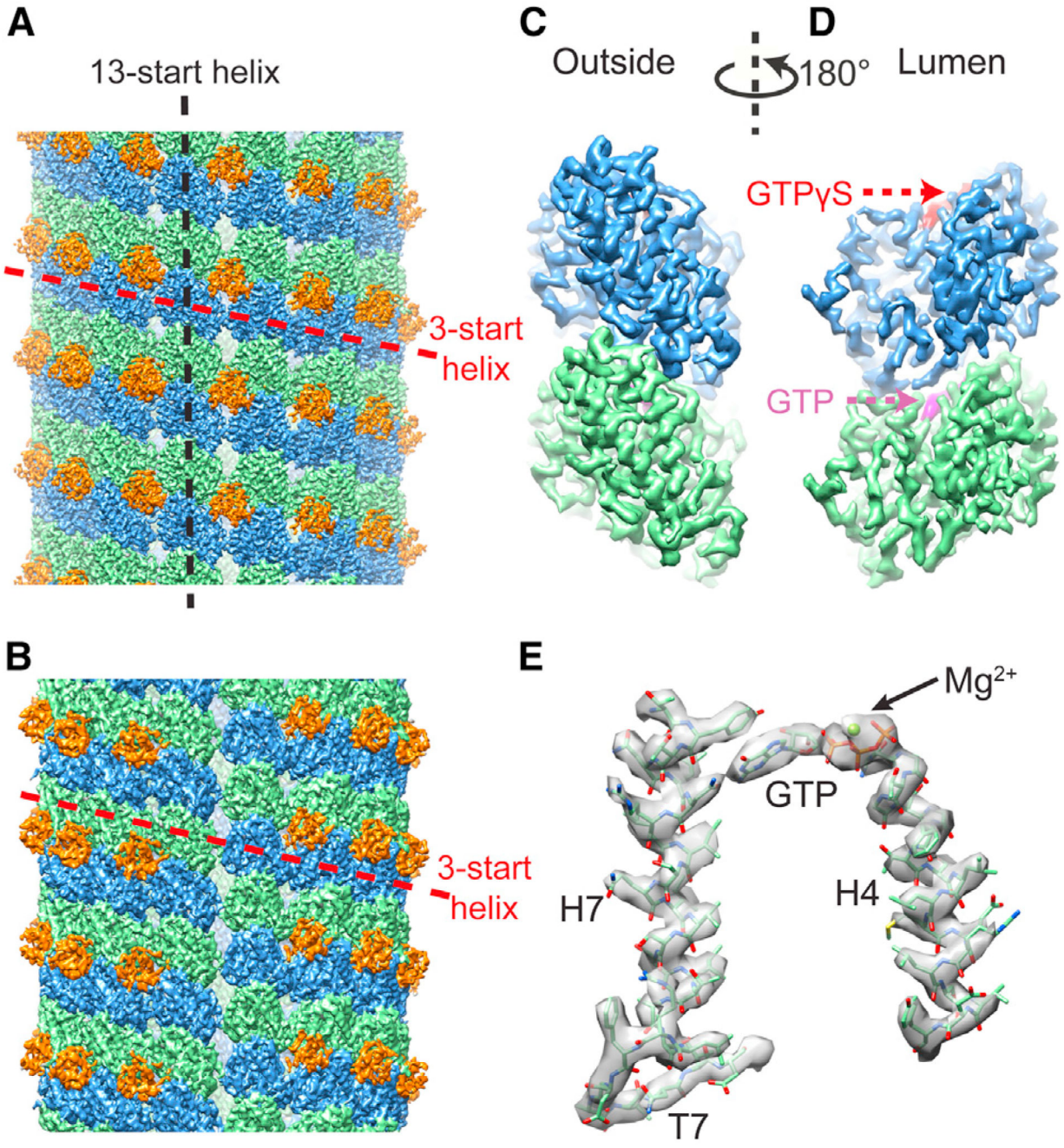

Figure 1. High-Resolution Cryo-EM Structure of EB3-Decorated GTPγS-MT

(A) Overview of the cryo-EM reconstruction of EB3-GTPγS-MT, with pseudo-helical symmetry applied. α-tubulin, β-tubulin and EB3 are colored green, blue and orange, respectively.

(B) The asymmetric (C1) reconstruction of (A) viewed from the seam.

(C and D) Density for an αβ-tubulin dimer segmented from a merged map of EB3-GTPγS-MT (with and without kinesin), viewed from the outside (C) and from the lumen (D) of the MT.

(E) Cryo-EM density segmented from (C) and atomic model of H4, H7 and T7 of α-tubulin, as well as the N-site GTP and coordinating Mg^{2+} ion.
See also Figure S1 and Tables S1 and S3.

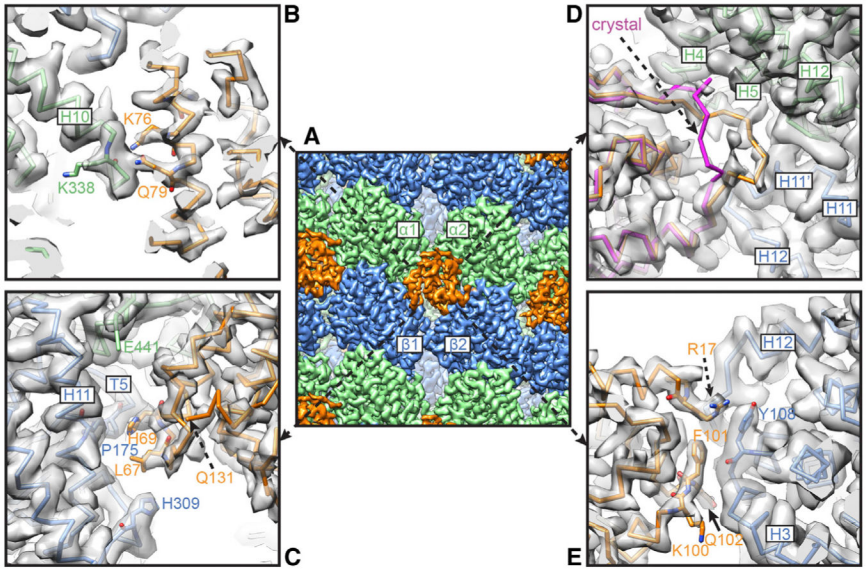

Figure 2. Interactions between the CH Domain of EB3 and the Four Tubulin Molecules It Contacts on the MT Surface

(A–E) Cryo-EM map (A) and models (B–E) of EB3-GTPγS-MT. Color scheme is the same as Figure 1. In (D) the crystal structure of EB3 (Protein Data Bank: 3CO1) is shown in magenta.

See also Figure S2 and Movie S2.

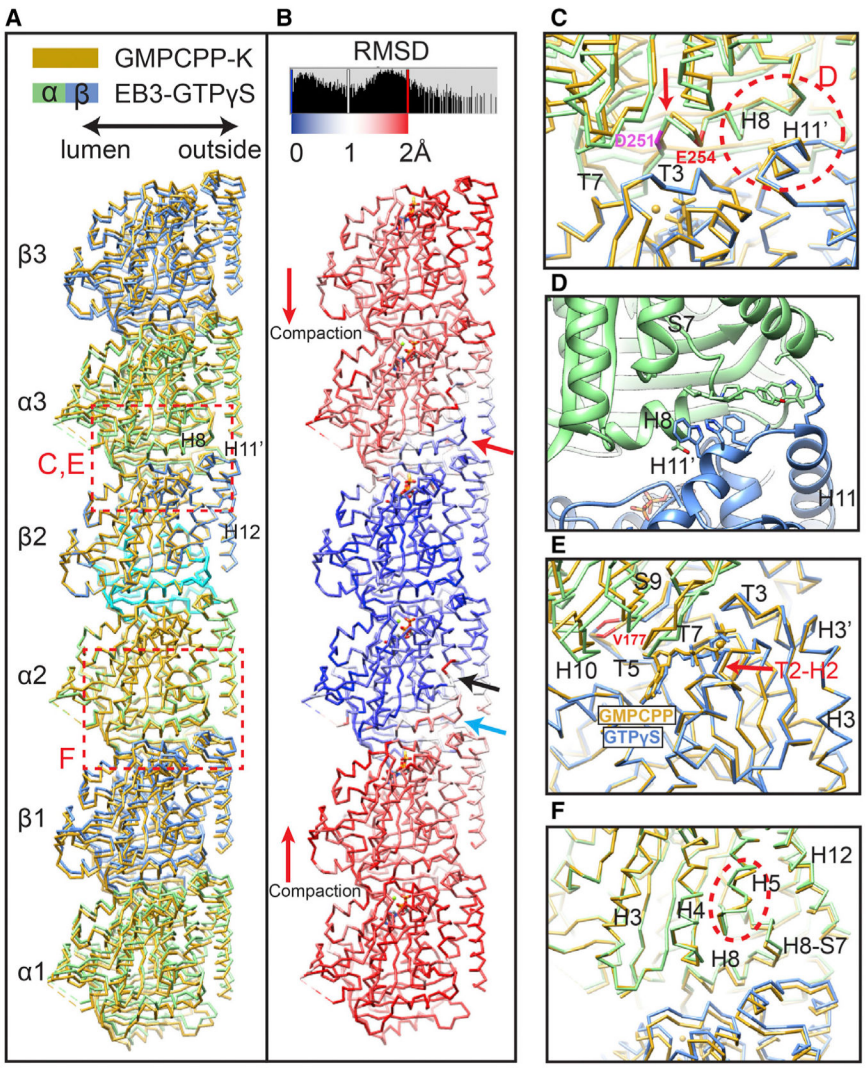

Figure 3. Lattice Compaction between the GMPCPP-K and EB3-GTPγS-MT States

(A) Comparison of the Cα traces of three consecutive tubulin dimers between the GMPCPP-K state (gold) and EB3-GTPγS state (green and blue for α- and β-tubulin, respectively), superimposed on the intermediate domain of β2-tubulin (cyan). Regions marked with red boxes are further visualized in the indicated panels.

(B) Cα-atoms-RMSD between the two models shown in (A), with deviations colored from blue to red (same for all figures). Features marked by arrows are further visualized in (C)–(G).

(C) Zoom-in view around the E-site. The red circle marks the position of the anchor point.

(D) Detailed view of the hydrophobic interactions at the anchor point.

(E) Same as (C), but from a different angle. Part of α-tubulin is hidden to improve clarity.

(F) Local change of the α:H5 helix.

See also Figures S3, S4, and S5, Table S2, and Movie S3.

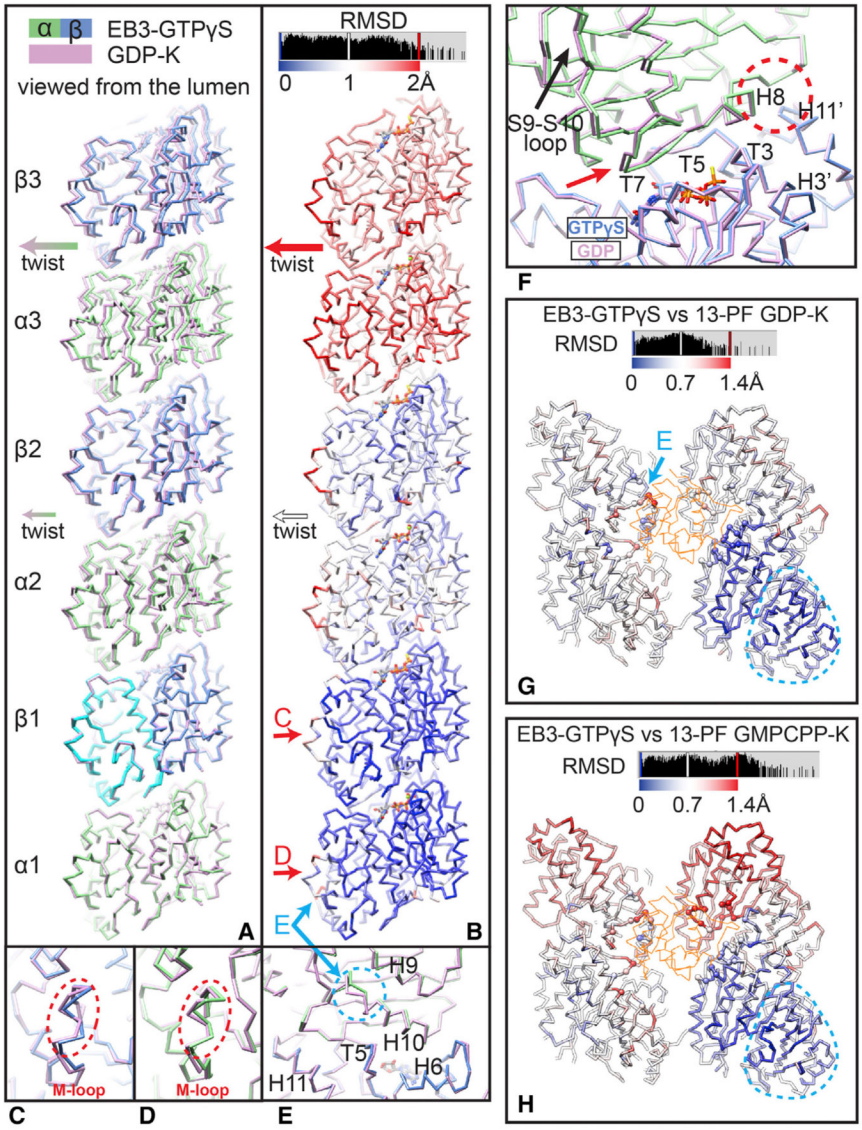

Figure 4. Lattice Twist between the EB3-GTPγS-MT and GDP-K-MT States

(A) Comparison of the Cα traces of three consecutive tubulin dimers between the EB3-GTPγS state (green and blue for α- and β-tubulin, respectively) and GDP-K state (light purple), superimposing on the intermediate domain of the bottom β1-tubulin (cyan) so that the lattice twist is more apparent in the top β3-α3 dimer.

(B) Cα-atoms-RMSD between the two models shown in (A). Differences marked by arrows are further visualized in (C)–(E).

(C and D) Changes of the M-loops of β-tubulin (C) and α-tubulin (D) due to the difference in PF number.

(E) Local change of the α:H10 helix likely due to EB3 binding.

(F) Zoom-in view around the E-site. Part of the α-tubulin is hidden to improve clarity. The red circle marks the position of the anchor point.

(G and H) Cα-atoms RMSD between the EB-binding pocket in the EB3-GTPγS-MT structure (13-PF) and the equivalent regions in the EB-free structures for (G) 13-PF GDP-K

and (H) 13-PF GMPCPP-K MTs. The models are superimposed on the intermediate domain of the bottom-right β-tubulin (cyan dashed circle), whose EB-contact region (H3′-H3 helices) does not move between all the EM structures analyzed. The Cα-atoms of tubulin residues that are within 5 Å distance from the EB3 CH domain (orange) are shown as balls. See also Figures S3, S4, and S5 and Table S2.

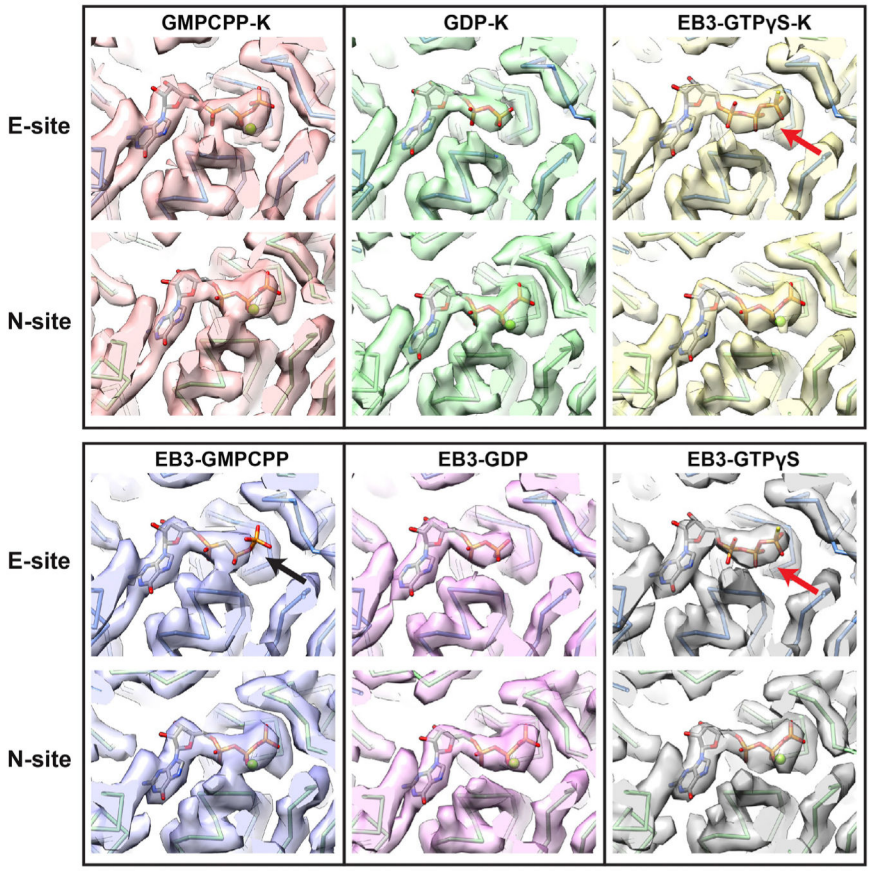

Figure 5. Densities and Atomic Models around the E-Site and N-Site Nucleotides for the Different MT Reconstructions

In all cases, the N-site displays clear density for both the γ-phosphate and the Mg^{2+} ion (green). Concerning the E-site, only the GMPCPP-K structure shows both the γ-phosphate and Mg^{2+} (top left panel), while both elements are missing in the GDP-K (top middle panel), EB3-GDP (bottom middle panel) and interestingly, the EB3-GMPCPP state (bottom left panel, black arrow). In the EB3-GTPγS structure (with and without kinesin, top right and bottom right panels), the γ-phosphate is clearly visible, while the Mg^{2+} ion is not present (red arrows).

See also Figure S3 and Tables S1 and S3.

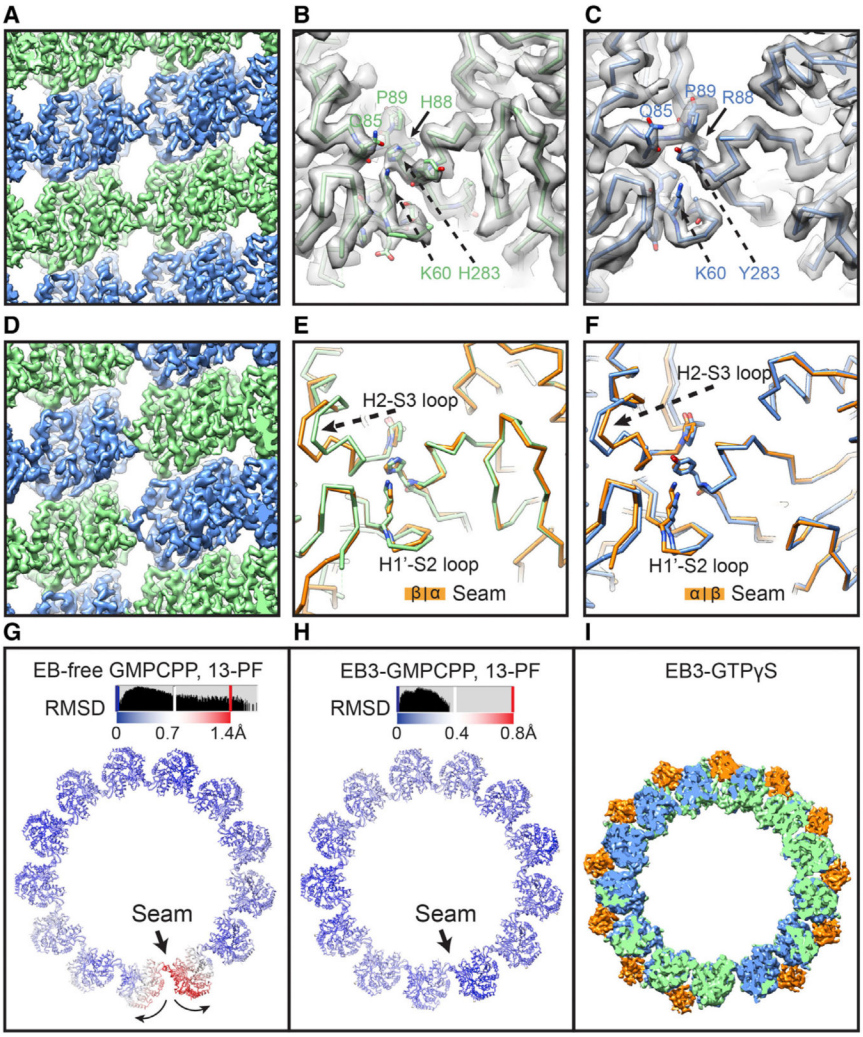

Figure 6. Lateral Interactions between Protofilaments

(A) Cryo-EM density map of merged EB3-GTPγS-MT (with and without kinesin) showing homotypic lateral interactions, viewed from the lumen side.

(B and C) Zoom-in view of the density and models of the α-α lateral interactions (B) and β-β lateral interactions (C).

(D) Cryo-EM density of the lateral interactions at the seam, obtained from the C1 reconstruction of the "EB-consensus" data.

(E and F) Comparisons of the atomic models for the lateral interactions between an α-β contact at the seam (orange) and a non-seam α-α contact (green) (E) or β-β contact (blue) (F).

(G and H) Cα-atoms RMSD between models of one helical turn of tubulin dimers for the C1 and the symmetrized reconstructions of the EB-free 13-PF GMPCPP-K-MT (G) and 13-PF EB3-GMPCPP-MT (H).

(I) The C1 reconstruction for the EB3-GTPγS-MT (same color scheme as Figure 1), viewed down along the MT axis.

See also Figures S6 and S7 and Movie S4.

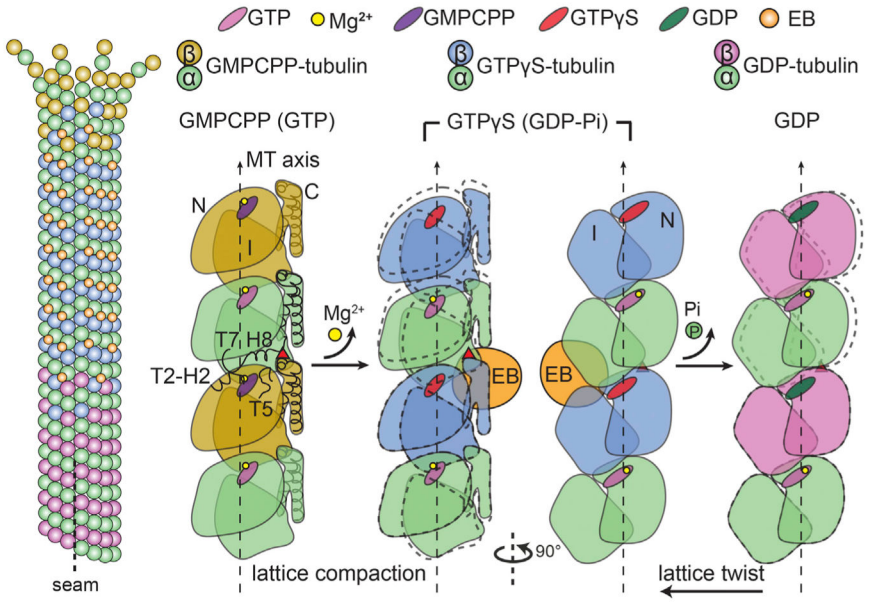

Figure 7. Schematic of the Conformational Changes Proposed to Accompany GTP Hydrolysis and the Effect of EB Proteins

α- and β-tubulin are illustrated as three domains (N-terminal, Intermediate and C-terminal). The red triangle at the tubulin interdimer interface indicates the anchor point during structural transitions. From GMPCPP (mimicking GTP) to GTPγS (mimicking GDP-Pi) state, changes around the E-site nucleotide (β:T2-H2, β:T5 and α:T7-H8) upon GTP hydrolysis and Mg^{2+} release accompany a lattice compaction at the interdimer interface (viewed from the side of the MT), with EB (orange) promoting and preferentially binding to the compacted intermediate GDP-Pi state. A subsequent change in lattice twist upon phosphate (Pi) release results in reduced of EB affinity (viewed from the lumen of the MT). See also Figure S3.